

Multi-mode chirped-Pearcey-Laguerre-Gaussian space-time wave packets synergistically regulated by dispersion and chirp

Yue Du(杜悦), Sai Ma(马赛), Chenchen Li(李晨晨), Haojie Li(李昊杰), Xiaolu Ge(葛筱璐), Chidao Chen(陈迟到), Benyi Wang(王本义), Zhongsheng Man(满忠胜), Wenfei Zhang(张文飞), and Liping Zhang(张丽萍)
Citation: Chin. Phys. B, 2026, 35 (**8**): 084210. DOI: 10.1088/1674-1056/ae64cf
http://cpb.iphy.ac.cn; http://iopscience.iop.org/cpb

What follows is a list of articles you may be interested in

Dual-wavelength polarization-tunable holographic response in an azobenzene-containing film

Hong Chen(陈红), Pan Wang(王潘), Ziyao Lyu(吕子瑶), and Changshun Wang(王长顺)
Chin. Phys. B, 2026, 35 (**5**): 054206. DOI: 10.1088/1674-1056/ae0b39

Highly sensitive, multi-stage, and mid-infrared refractive index sensor based on photonic spin Hall effect

Jiaye Ding(丁嘉烨), Chenglong Wang(汪承龙), Shengli Liu(刘胜利), Peng Dong(董鹏), and Jie Cheng(程杰)
Chin. Phys. B, 2026, 35 (**1**): 014201. DOI: 10.1088/1674-1056/ade24c

Fusion of fractional vortex pairs and their transition to integer vortex controlled by optical power

Chunzhi Sun(孙春志), Xiangwei Chen(陈向炜), Huizhong Xu, and Guo Liang(梁果)
Chin. Phys. B, 2025, 34 (**5**): 054202. DOI: 10.1088/1674-1056/adb8b9

Surface phonon resonance: A new mechanism for enhancing photonic spin Hall effect and refractive index sensor

Jie Cheng(程杰), Chenglong Wang(汪承龙), Yiming Li(李一铭), Yalin Zhang(张亚林), Shengli Liu(刘胜利), and Peng Dong(董鹏)
Chin. Phys. B, 2024, 33 (**8**): 084201. DOI: 10.1088/1674-1056/ad4a3c

Multi-functional photonic spin Hall effect sensor controlled by phase transition

Jie Cheng(程杰), Rui-Zhao Li(李瑞昭), Cheng Cheng(程骋), Ya-Lin Zhang(张亚林), Sheng-Li Liu(刘胜利), and Peng Dong(董鹏)
Chin. Phys. B, 2024, 33 (**7**): 074203. DOI: 10.1088/1674-1056/ad3b85

Multi-mode chirped-Pearcey–Laguerre–Gaussian space–time wave packets synergistically regulated by dispersion and chirp

Yue Du(杜悦)[1], Sai Ma(马赛)[1], Chenchen Li(李晨晨)[1], Haojie Li(李昊杰)[1], Xiaolu Ge(葛筱璐)[1], Chidao Chen(陈迟到)[2], Benyi Wang(王本义)[1], Zhongsheng Man(满忠胜)[1], Wenfei Zhang(张文飞)[1,†], and Liping Zhang(张丽萍)[1,‡]

[1] *School of Physics and Optoelectronic Engineering, Shandong University of Technology, Zibo* 255000, *China*
[2] *School of Medical Imaging, Qilu Medical University, Zibo* 255300, *China*

(Received 22 January 2026; revised manuscript received 20 April 2026; accepted manuscript online 27 April 2026)

This study introduces the chirped-Pearcey–Laguerre–Gaussian space–time (CPLGST) wave packets and investigates their propagation characteristics in linear dispersive media, uncovering diverse propagation regimes of the CPLGST wave packets as the radial and angular mode numbers are tuned. Modulating the second-order chirp factor and dispersion coefficient allows for tailored manipulation of the envelope profile, evolution trajectory, and propagation dynamics of the CPLGST wave packets. It further uncovers the dynamic balance regulation mechanism of the CPLGST wave packets, which is mediated by the synergistic effect of the second-order chirp factor and dispersion coefficient, while also examining the evolution characteristics and peak intensity variation laws of such wave packets under normal and anomalous dispersion conditions. Additionally, this study explores the gradient and scattering force characteristics of the CPLGST wave packets, thereby further exploring their potential applications in optical tweezers technology and microparticle manipulation.

Keywords: space–time wave packets, linear dispersive media and optical forces

PACS: 42.25.–p, 42.50.Wk

DOI: 10.1088/1674-1056/ae64cf **CSTR:** 32038.14.CPB.ae64cf

1. Introduction

In recent years, novel structured optical fields have emerged as a prominent research focus in optics.[1,2] Structured light plays a pivotal role in optical trapping technology,[3,4] and also lays a theoretical and physical foundation for investigating intense laser-induced molecular dynamics.[5] In the field of biomedicine, it offers technical feasibility for single-cell capture and multi-cell arrangement.[4] Furthermore, high-dimensional structured light not only enables ultra-high-speed and long-distance transmission in the field of communication but also facilitates the construction of high-dimensional quantum networks in quantum science, thereby enhancing communication security and transmission efficiency.[2,6,7] As a paradigmatic class of structured beams, Laguerre–Gaussian (LG) beams have attracted extensive research interest. In 1992, Allen and his colleagues first proposed that LG beams possess quantifiable orbital angular momentum (OAM),[8] while elaborating on the specific conversion mechanism between beam modes and angular momentum. This theoretical proposition was subsequently validated through experimental investigations.[9,10] Owing to their inherent OAM, LG beams exert optical torques in optical tweezers, inducing rotational or translational motion of trapped particles,[8,11] a property that confers on them substantial application potential in optical tweezers technology and micro-particle manipulation.[12–14] Subsequently, Airy beams[15,16] and Pearcey beams[17,18] were successively proposed, and research efforts have continued to advance toward enhancing the self-focusing capabilities of these two beam types.[19–23] Building on this foundation, a series of derivative beams derived from Airy and Pearcey beams have been developed,[24–26] thereby further enriching the theoretical framework of emerging structured light fields.

Research on novel structured optical fields has expanded beyond the traditional spatial domain into the temporal realm, with extensive explorations conducted on space–time wave packets (STWPs).[27–29] A series of innovative beam-based wave packet studies has been reported successively, including Airyprime complex-variable-function wave packets,[30] symmetric Pearcey–Pearcey wave packets,[31] and Airyprime–Laguerre–Gaussian wave packets.[32] In the context of structured light research, the application scope of STWPs in trajectory control and dynamic manipulation has been continuously extended. Notable examples include LG wave packets endowed with the capability of self-acceleration and self-focusing along preset trajectories,[33] STWPs with arbitrarily tailorable propagation trajectories,[34] and Pearcey–Gaussian wave packets realized through "fly-focus" technology,[35] all of which exhibit distinct functional advantages in trajectory manipulation. However, Pearcey–Laguerre–Gaussian spa-

†Corresponding author. E-mail: zhangwenfei@sdut.edu.cn
‡Corresponding author. E-mail: jpzhang@sdut.edu.cn

© 2026 Chinese Physical Society and IOP Publishing Ltd. All rights, including for text and data mining, AI training, and similar technologies, are reserved.

tiotemporal wave packets need to be further studied. To tackle this research gap, we propose chirped-Pearcey–Laguerre–Gaussian space–time wave packets (CPLGST), aiming to systematically investigate their spatiotemporal characteristics and dispersion behaviors while exploring their potential in optical trapping and particle manipulation.

Based on the linear Schrödinger equation and the method of separation of variables, this study constructs the CPLGST wave packets via the integration of the time-domain chirped Pearcey and the spatial-domain LG beams. The three-dimensional propagation characteristics of the CPLGST wave packets are visualized through a comprehensive propagation diagram, with the underlying mechanism governing how the second-order chirp and dispersion coefficient influence the dispersion behavior of the wave packets being systematically unraveled. It is demonstrated that the second-order chirp factor induces wave packet splitting, with the evolutionary process of the wave packets from "envelope–split–envelope" comprehensively depicted. Furthermore, the effects of normal and anomalous dispersion on the wave packets' structure are explored, and the cooperative interaction mechanism of the dispersion coefficient and the second-order chirp factor on the wave packets is clarified. Ultimately, the distribution characteristics of the gradient force and scattering force under different mode numbers are analyzed.

2. Theoretical formulation of the CPLGST

The propagation of the CPLGST wave packets can be expressed by the linear Schrödinger equation, and its normalized form under the paraxial approximation condition is[31,36]

$$\mathrm{i}\frac{\partial u}{\partial Z}+\frac{1}{2k}\left(\frac{\partial^2}{\partial X^2}+\frac{\partial^2}{\partial Y^2}\right)u-\frac{k_{\mathrm{o}}''}{2}\frac{\partial^2 u}{\partial T^2}=0, \tag{1}$$

where $u(X,Y,Z,T)$ is the complex amplitude envelope, $X=x/w, Y=y/w$ are normalized coordinates (w is the waist of the beam), and $T=t-\frac{z}{v_{\mathrm{g}}}$ corresponds to the time in a reference frame traveling with the group velocity v_{g} of the wave. $k=\omega_0 n(\omega_0)/c$ represents the wave number, c describes the speed of light, $n(\omega_0)$ describes the index of refraction, ω_0 represents the centre frequency ($\omega_0=2\pi c/\lambda$), λ describes the central wavelength of the wave packets, and $k_{\mathrm{o}}''=\partial^2 k/\partial\omega_0^2$ represents the influence of the group velocity dispersion (GVD).[36] The dispersion coefficient β is used to represent k_{o}'', and $\mathrm{sign}(\beta)=+1/-1$ corresponds to normal/abnormal GVD. The propagation coordinate Z is normalized by the dispersion length L_{d}. In the present study, we postulate that $L_{\mathrm{d}}=T_0^2/|\beta|$.[37] T_0 represents the initial pulse width of the CPLGST wave packets. We decompose the CPLGST wave packets into a coupled form of spatial Laguerre beams and time-domain chirped Pearcey pulses using the separation of variables method:[31–33]

$$u(X,Y,Z,T)=\Psi(X,Y,Z)\Theta(Z,T). \tag{2}$$

By substituting Eq. (2) into Eq. (1), we derive the following two differential equations:[36]

$$\mathrm{i}\frac{\partial\Theta}{\partial Z}-\frac{k_{\mathrm{o}}''}{2}\frac{\partial^2\Theta}{\partial T^2}=0, \tag{3}$$

$$2\mathrm{i}\frac{\partial\Psi}{\partial Z}+\frac{1}{k}\left(\frac{\partial^2}{\partial X^2}+\frac{\partial^2}{\partial Y^2}\right)\Psi=0. \tag{4}$$

For Eq. (3), we use the chirped Pearcey pulse as the initial condition. The incident field on the initial plane ($Z=0$) is expressed as

$$\Theta(0,T)=Pe(\tau,T)\,\mathrm{e}^{\left(\alpha T+\mathrm{i}C_1T+\mathrm{i}C_2T^2\right)}. \tag{5}$$

Here, the Pearcey function is defined as $Pe(X,Y)=\int_{-\infty}^{+\infty}\exp\left(\mathrm{i}s^4+\mathrm{i}Xs+\mathrm{i}Ys^2\right)$.[22,23,25] α represents the attenuation factor ($0<\alpha<1$), C_1 and C_2 are the first-order chirp factor and the second-order chirp factor, τ denotes the temporal scaling parameter for the Pearcey function, and we set $\tau=10$. $\Psi(X,Y,0)$ represents the Laguerre–Gaussian beam that can be defined as follows:[33,38]

$$\begin{aligned}\Psi(X,Y,0)&=\left(\sqrt{2X^2+2Y^2}\right)^l L_n^l(2X^2+2Y^2)\\&\quad\times\exp(-X^2-Y^2+\mathrm{i}l\theta),\end{aligned} \tag{6}$$

$$L_n^l(x)=\sum_{m=0}^{l}\frac{(-x)^m(l+n)^m}{(m+l)!\,(n-m)!m!}. \tag{7}$$

In the present context, n and l correspond to the radial mode number and angular mode number, $\theta=\tan^{-1}(Y/X)$.

We employ the step-by-step Fourier method to simulate the propagation process and analyze $\Theta(Z,T)$ and $\Psi(X,Y,T)$ to investigate the characteristics of the CPLGST wave packets. The gradient force and scattering force of the CPLGST wave packets can be expressed by the following formula:[39–41]

$$F_{\mathrm{gard}}=\frac{2\pi n_2 r^3}{c}\left(\frac{\eta^2-1}{\eta^2+2}\right)\nabla I(X,Y,Z), \tag{8}$$

$$F_{\mathrm{scat}}=\frac{8\pi n_2 k^4 r^6}{3c}\left(\frac{\eta^2-1}{\eta^2+2}\right)I(X,Y,Z)\overrightarrow{e_z}, \tag{9}$$

$$I(x,y,z)=cn_2\varepsilon_0\frac{|u(x,y,z)|^2}{2}. \tag{10}$$

The r represents the radius of the nanoparticle, $\eta=n_1/n_2$ is the relative refractive index, where n_1 represents the refractive index of the particle, and n_2 is the refractive index of the surrounding medium. ∇ represents the gradient operator, ε_0 is the permittivity of the free space, and the intensity $I(x,y,z)$ is the light intensity of the CPLGST wave packets. In this article, we set $\lambda=532$ nm, $w=1$ mm, $\alpha=0.2$, $T_0=1$ ps, $n_1=1.592$, and $n_2=1$. Unless otherwise specified, the value of β is 2×10^{-25}.

It should be emphasized that the paraxial approximation and linear Schrödinger model adopted in this study are only valid within moderate parameter regimes. The theoretical

framework may break down under several extreme conditions, including wave packets carrying excessively high mode orders or large topological charges, dispersion values far exceeding the range employed in the present work, and ultrashort pulses with an ultrabroad spectral bandwidth. Since all parameters in this study are constrained within a reasonable and valid range, the above limiting effects are negligible, thus guaranteeing the reliability and accuracy of the theoretical analysis.

3. Results and discussion

To investigate the effect of the radial mode number on the propagation characteristics of the CPLGST wave packets, we fixed a single angular mode number and systematically characterized the evolution behavior of the CPLGST wave packets at different positions throughout their propagation. As shown by the two-dimensional propagation characteristics in Fig. 1, the beam exhibits highly concentrated spatial intensity during the initial propagation stage. In the X–Z plane, the constructive interference of multiple radial modes with tailored phase relations effectively inhibits near-field diffraction-induced beam broadening. The beam maintains uniform, equidistant fringes, accompanied by negligible phase distortion and energy migration. This observation further confirms the near-field propagation invariance of the CPLGST wave packets. Only after propagating a certain distance does the beam intensity undergo non-uniform decay. Diffusion starts from the edge of the light spot, and the well-defined boundaries gradually fade. This demonstrates that the accumulated phase difference among radial modes breaks the coherent superposition required for propagation invariance, which eventually induces energy divergence and intensity attenuation. A comparison of Figs. 1(A) and 1(B) reveals that a greater radial mode number corresponds to a more dispersed radial energy distribution. This dispersion arises because higher-order radial modes introduce additional high-order spatial frequency components in the transverse plane, thereby broadening the radial intensity distribution and reducing the central energy concentration. For comparative purposes, we further present the three-dimensional spatiotemporal intensity distributions of the CPLGST wave packets at different propagation positions in Figs. 1(a1)–1(a3) and 1(b1)–1(b3). The CPLGST wave packets assume an overall concentric circular ring envelope. In the X–Y plane projection, intensity is most concentrated at the spatial center and diminishes radially outward. A lateral comparison of Figs. 1(a1)–1(a3) shows that the central envelope of the CPLGST wave packets compresses, the intensity of the CPLGST wave packets attenuates, and the concentric ring structure of the CPLGST wave packets expands to cover a broader morphological evolution. A vertical comparison of the CPLGST wave packets with different radial mode numbers, as depicted in Figs. 1(a1)–1(a3) and 1(b1)–1(b3), clearly demonstrates that a greater radial mode number yields more concentric rings and a wider spatial coverage. In summary, reducing the radial mode number can enhance the energy concentration of the CPLGST wave packets, significantly improving their focusing characteristics while also enabling propagation invariance over a specific morphological evolution. The CPLGST wave packets achieve a longer propagation-invariant distance of 5–7.5L_d, superior to the 3–4L_d of standard Laguerre–Gaussian wave packets, and avoid the random broadening of Airy wave packets for more stable propagation.[42]

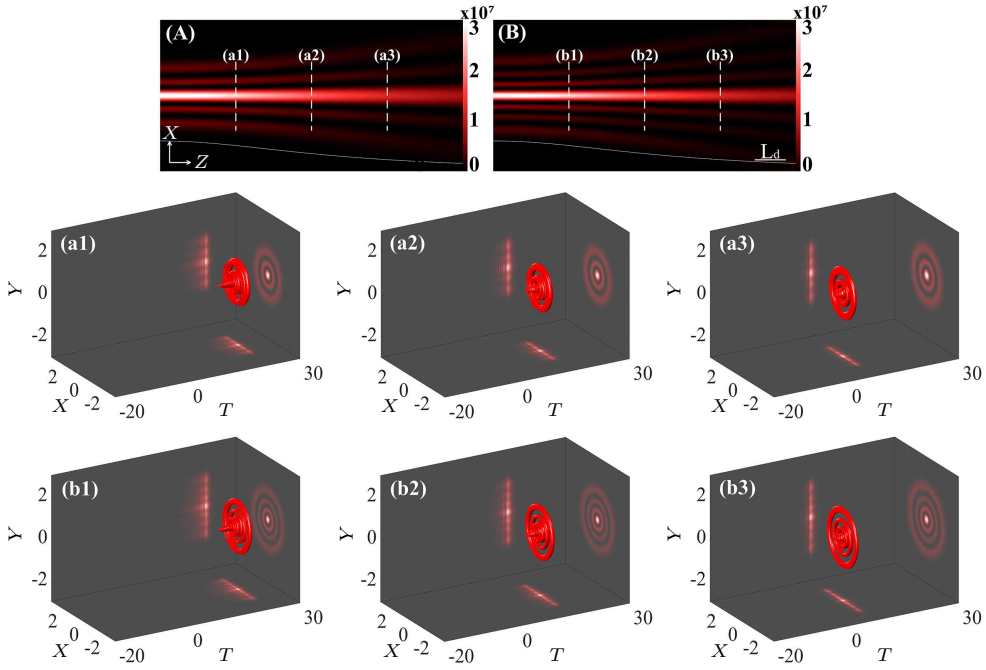


Fig. 1. (A) and (B) are the numerical side views of the propagation of the CPLGST wave packets, while (a1)–(a3) and (b1)–(b3) are the spatiotemporal transmission maps at different propagation positions. $C_1 = 0.5$, $C_2 = 0.5$, $Z = 2.5L_d$ in (a1) and (b1), $Z = 5L_d$ in (a2) and (b2), $Z = 7.5L_d$ in (a3) and (b3), $n = 2$, $l = 0$ in (A) and (a1)–(a3), and $n = 3$, $l = 0$ in (B) and (b1)–(b3).

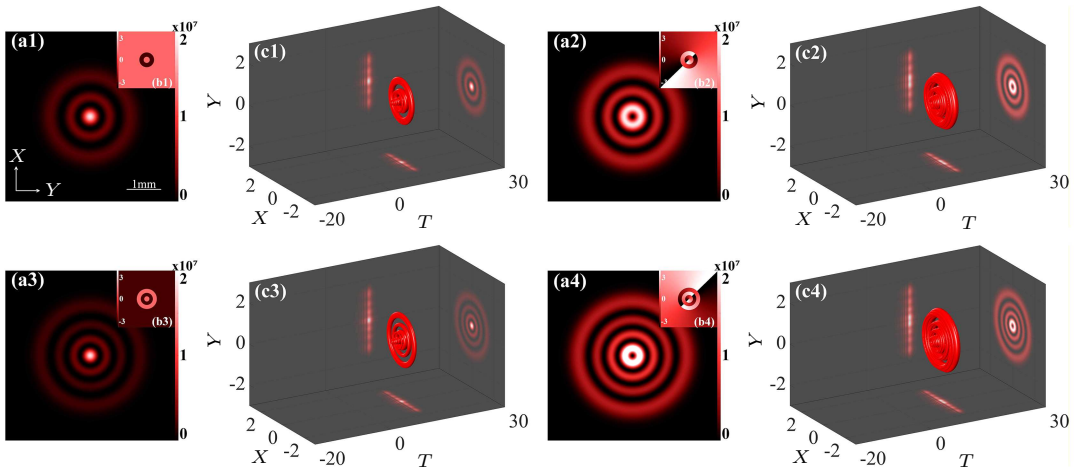


Fig. 2. (a1)–(a4) are the transverse intensity patterns, (b1)–(b4) are the phase distributions under the corresponding parameters, and (c1)–(c4) are the corresponding wave packets of CPLGST. The parameters are as follows: $Z = 5L_{\mathrm{d}}$, $C_1 = 0.6$, $C_2 = 0.6$, $n = 2$, $l = 0$ in (a1)–(c1), $n = 2$, $l = 1$ in (a2)–(c2), $n = 3$, $l = 0$ in (a3)–(c3), and $n = 3$, $l = 1$ in (a4)–(c4).

Subsequently, we systematically characterize the initial optical fields, phase distribution, and the CPLGST wave packets of configurations with distinct radial and angular modes. We first assess the impact of the radial mode. The initial optical field exhibits a concentric circular structure with a bright central region and dark outer rings, and the number of outer dark rings increases with the radial mode number. As illustrated in Fig. 2(a3), the radial optical field exhibits a more densely layered ring-shaped distribution than that in Fig. 1(a1), with each ring also possessing a more compact width. The notable increase in radial spatial filling of the optical field clearly indicates that the radial mode number is the key parameter determining the number of radial rings within the field. We then vary the angular mode number to study its effects on the optical field. The originally compact central bright spot gradually expands into a closed central bright ring. Additionally, direct comparison reveals that the central bright spot in Fig. 2(a2) is brighter than that in Fig. 2(a1). Furthermore, a direct comparison of Figs. 2(c1) and 2(c2) reveals that increasing angular mode number strengthens the helical structural characteristics of the CPLGST wave packets. This enhancement leads to a more distinct helical direction, a more uniform pitch, and a significant elongation of the CPLGST wave packets' envelope along the time dimension. This variation reveals that the angular mode number is closely related to the optical field OAM. Increasing the angular mode number yields a higher OAM and a sharper spiral phase gradient, which strengthens the wave packets' spiral configuration and spatiotemporal coupling behavior during propagation. There exists a fixed phase difference $\Delta\theta = \arctan(Y/X)$ between Laguerre modes corresponding to different radial and azimuthal mode numbers. Their interference directly modulates the number and intensity distribution of the bright rings of the wave packets, and the uniformity of the phase difference ensures the integrity of the spatial structure after the wave packets are formed by interference, with no extraneous bright rings and thus no degradation of the wave packet quality. In contrast, the spatiotemporal coupled evolution is dominated by the synergistic effect of the second-order chirp factor and the dispersion coefficient, whose numerical matching regulates the phase coupling strength in the spatiotemporal domain and further determines the evolution trajectory and morphology of the wave packets. Regarding the structural transition stability of the wave packets during the switching of radial and azimuthal mode numbers, Fig. 2 intuitively illustrates this issue, and other key parameters were fixed during mode switching to avoid introducing additional effects. The phase modulation depth is directly related to the azimuthal mode number l and the phase term $\mathrm{i}l\theta$. Within the same modulation scheme, quantitative variation of l only changes the phase rotation rate without destroying the consistency of the phase modulation depth, thus guaranteeing the stable evolution of the wave packets' structure under different mode numbers. By cross-comparing the initial optical fields and the CPLGST wave packets under different mode parameters, we establish that the radial and angular mode numbers synergistically regulate the initial optical field structure and the evolution characteristics of the CPLGST wave packets. Jointly, these two parameters provide a critical foundation for mode-based modulation of the CPLGST wave packets. This foundational support enables precise regulation of the radial annular parameters and the helical structures of the angular CPLGST wave packets, which in turn enables the targeted utilization of these wave packets in optical manipulation and information transmission applications.

In Fig. 3, we uncover the effect of the second-order chirp factor on the propagation dynamics of the CPLGST wave packets by tuning this parameter systematically. As the second-order chirp factor increases, the spatial position of the CPLGST wave packets shifts gradually from right to left, accompanied by a distinctive splitting phenomenon. When the second-order chirp factor is approximately 0.8, as depicted

in Figs. 3(a2) and 3(b2), the CPLGST wave packets initially adopt a concentric circular structure in the spatiotemporal domain that then undergoes dynamic evolution during propagation, ultimately splitting into two spatially isolated and nearly symmetric sub-wave packet units. The physical origin of this phenomenon lies in the critical equilibrium established between the second-order chirp factor and GVD. At this threshold, the frequency component separation induced by GVD exactly overcomes the confinement of the pulse envelope, giving rise to the CPLGST wave packets splitting. When the second-order chirp factor takes smaller values, frequency components remain confined by the pulse envelope, leading merely to trivial pulse broadening instead of the characteristic CPLGST wave packets splitting. Conversely, for an excessively great chirp factor, the dispersion-driven separation cannot match the rate of envelope contraction, and the CPLGST wave packets re-converge into a concentric circular configuration. Thus the CPLGST wave packets also exhibit self-healing properties. Moreover, a cross-comparison of Figs. 3(a1)–3(a3) and 3(b1)–3(b3) shows that propagation distance modulates the spatiotemporal evolution of the CPLGST wave packets when the second-order chirp factor is held fixed. As propagation distance increases, energy initially concentrated in the central region disperses progressively, leading to a flatter CPLGST wave packet profile and more uniform energy distribution across the spatial domain. We combine the propagation characteristics of linear dispersive media with the requirements for controllable wave packet evolution to determine their effective regulation ranges: the second-order chirp factor must satisfy $0 < C_2 < 1.5$. If $C_2 \leq 0$, the wave packets exhibit no chirp modulation effect and cannot be triggered to undergo splitting. If $C_2 \geq 1.5$, the spectral components undergo irreversible separation due to excessive chirping, and the wave packets lose the controllable evolution properties of self-convergence and self-repair. The dispersion coefficient is chosen on the order of 10^{-25}–10^{-24}. If the dispersion coefficient β is too small, the dispersion effect becomes negligible and cannot synergistically interact with the chirp factor. If it is too large, dispersion dominates the wave packet evolution; the regulatory effect of chirp is masked, and the wave packets undergo irregular broadening. In practical experiments, the modulation error of the second-order chirp factor should be controlled within ± 0.05. This precision threshold is determined by the threshold condition for wave packet splitting: in this study, $C_2 \approx 0.8$ corresponds to the critical value for wave packet splitting. If the modulation error exceeds ± 0.05, the critical condition will be directly violated, leading to incomplete splitting or premature convergence of the wave packets, thereby destroying the controllability of the evolution trajectory. This study focuses on the characteristics of CPLGST wave packets in linear dispersive media, with the selected light intensity $I < 10^7$ W/m^2, and all modulation parameters lying within the linear optical regime. The nonlinear polarization effect of the medium can thus be neglected, so that no nonlinear distortion of the wave packets occurs. To conclude, the second-order chirp factor and propagation distance synergistically govern the spatiotemporal evolution of the CPLGST wave packets, with a dynamic balance existing between the chirp factor and GVD throughout this process. This result furnishes a critical theoretical framework for the precise control of the CPLGST wave packet evolution behavior.

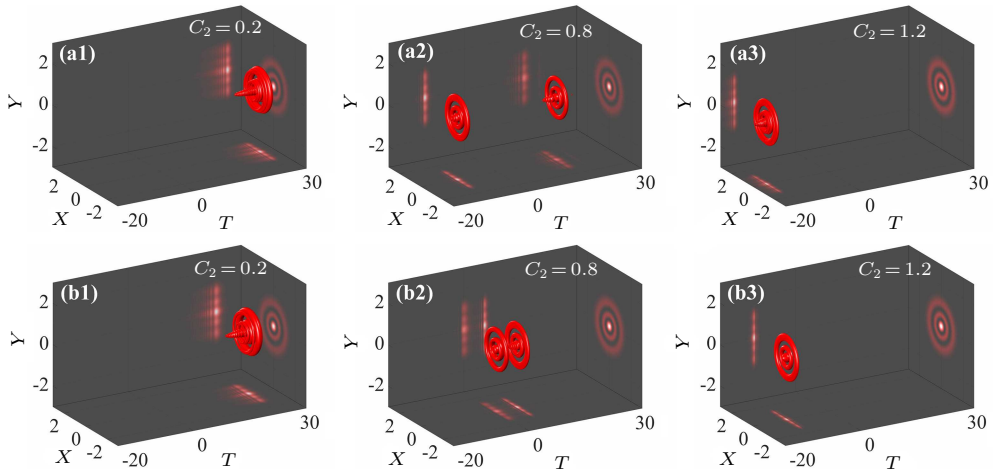


Fig. 3. (a1)–(a3) and (b1)–(b3) The CPLGST wave packets under the control of different second-order chirp factors. The parameters are as follows: $n = 2$, $l = 0$, $C_1 = 0$. (a1)–(a3) are the CPLGST wave packets corresponding to $Z = 2.5L_{\mathrm{d}}$. (b1)–(b3) correspond to $Z = 5L_{\mathrm{d}}$.

Dispersion constitutes a critical factor governing the morphological evolution of the CPLGST wave packets; to uncover its regulatory mechanism, we systematically studied the impact of dispersion on the propagation characteristics of the CPLGST wave packets in Fig. 4. Under normal dispersion conditions, as depicted in Figs. 4(a1) and 4(b1), the helical structure of the CPLGST wave packets exhibits enhanced compactness, with the projected light spot remaining highly

concentrated. Contrastingly, under anomalous dispersion conditions, as shown in Fig. 4(a2) and 4(b2), the helical structure of the CPLGST wave packets stretches longitudinally along the time axis and diffuses spatially, leading to the formation of periodic striped projections. Physically, normal dispersion enforces an ordered temporal arrangement of the frequency components of the CPLGST wave packets, where the helical "rotation direction" aligns with the dispersion orientation to preserve structural stability. A vertical comparison reveals that the dispersion strength at $\beta = 6 \times 10^{-25}$ is higher than that at $\beta = 2 \times 10^{-25}$; accordingly, the helical structures in Figs. 4(a1) and 4(a2) are more compact and have more concentrated energy than those in Figs. 4(b1) and 4(b2). Interestingly, low-frequency components of the CPLGST wave packets propagate ahead of high-frequency components under normal dispersion conditions. As dispersion strength increases, cumulative dispersion effects allow high-frequency components to overtake low-frequency ones, which triggers a reversal in the propagation direction of the wave packets. This phenomenon indicates that when the dispersion-induced group velocity difference accumulates to a critical threshold, the relative propagation sequence of different frequency components reverses, ultimately altering the macroscopic propagation direction of the wave packet. This mechanism provides a new physical degree of freedom for the dynamic manipulation and regulation of spatiotemporal wave packets. Collectively, these results demonstrate that both the normal or anomalous dispersion and its magnitude synergistically modulate the spatial architecture, extension degree, and propagation direction of the CPLGST wave packets. This insight further enables the tailored selection of dispersive materials to achieve desired beam broadening or compression, thereby furnishing a novel framework for the temporal control of optical beams.

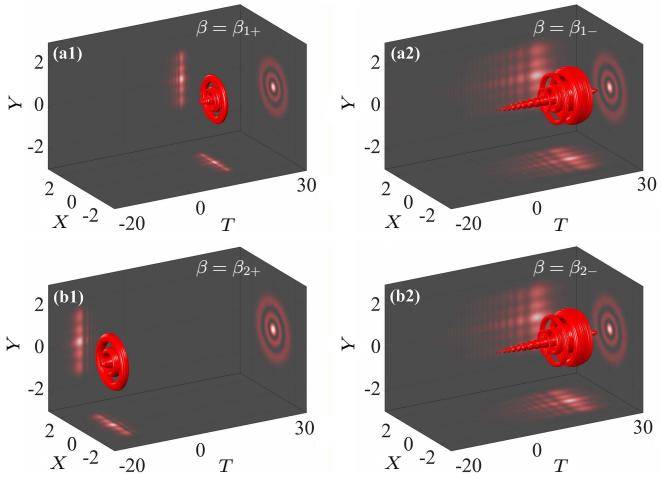


Fig. 4. (a1)–(a2) and (b1)–(b2) Space–time transmission diagrams of the CPLGST wave packets at $Z = 5L_d$. $C_1 = 0$, $C_2 = 0.5$, $n = 2$, $l = 0$, $\beta_{1+} = 2 \times 10^{-25}$, $\beta_{1-} = -2 \times 10^{-25}$, $\beta_{2+} = 6 \times 10^{-25}$, and $\beta_{2-} = -6 \times 10^{-25}$.

By harnessing the intensity side view within the X–T plane, we delineate the propagation dynamics of the CPLGST wave packets modulated by the synergistic interplay of dispersion and the second-order chirp factor. A systematic analysis of the results from Fig. 5 reveals that the propagation direction of the CPLGST wave packets is immediately determined by the product of the dispersion factor and the second-order chirp factor. When the product of the dispersion factor and the second-order chirp factor is negative, as shown in Figs. 5(b) and 5(c), CPLGST wave packets propagate in the positive direction along the T-axis. They exhibit an elongated, periodic spatiotemporal distribution, with their light intensity stretched into dense oscillatory stripes in the time dimension. In contrast, when the product is positive, as demonstrated in Figs. 5(a) and 5(d), the propagation direction of the wave packets reverses. In turn, the wave packets take on a compact, spatially confined distribution with high-intensity, tightly focused peaks emerging within limited spatiotemporal domains. Remarkably, under anomalous dispersion conditions with a negative second-order chirp factor, the peak light intensity of the CPLGST wave packets increases significantly, while this trend is completely reversed under normal dispersion conditions. These observations confirm that the second-order chirp factor and dispersion factor jointly modulate the temporal evolution of the CPLGST optical pulses via synergistic interactions between their sign characteristics and numerical coupling. This regulatory mechanism not only governs the propagation direction and spatiotemporal distribution morphology of the CPLGST wave packets but also affects the degree of light intensity concentration, thereby providing critical theoretical support for the development of high-power laser pulse generation applications.[43] Unlike conventional Laguerre–Gaussian, Airy, and Pearcey-based wave packets with monotonically attenuated peak intensity, the CPLGST wave packets feature lower attenuation and realizable directional intensity enhancement via chirp–dispersion coupling.[44]

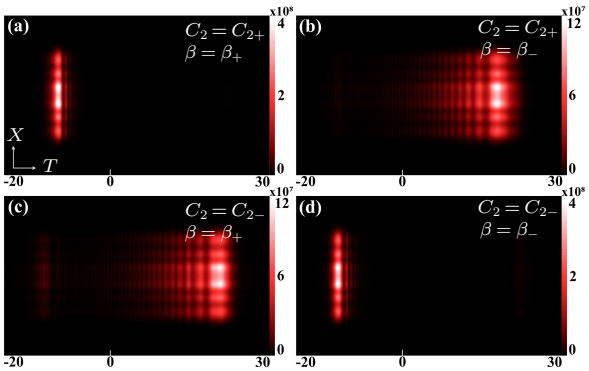


Fig. 5. (a)–(d) The side view of the space–time intensity of the CPLGST wave packets in the dimension of time at $Z = 5L_d$. $n = 2$, $l = 2$, $C_1 = 0$, $C_{2+} = 0.7$, $C_{2-} = -0.7$, $\beta_+ = 2 \times 10^{-25}$, and $\beta_- = -2 \times 10^{-25}$.

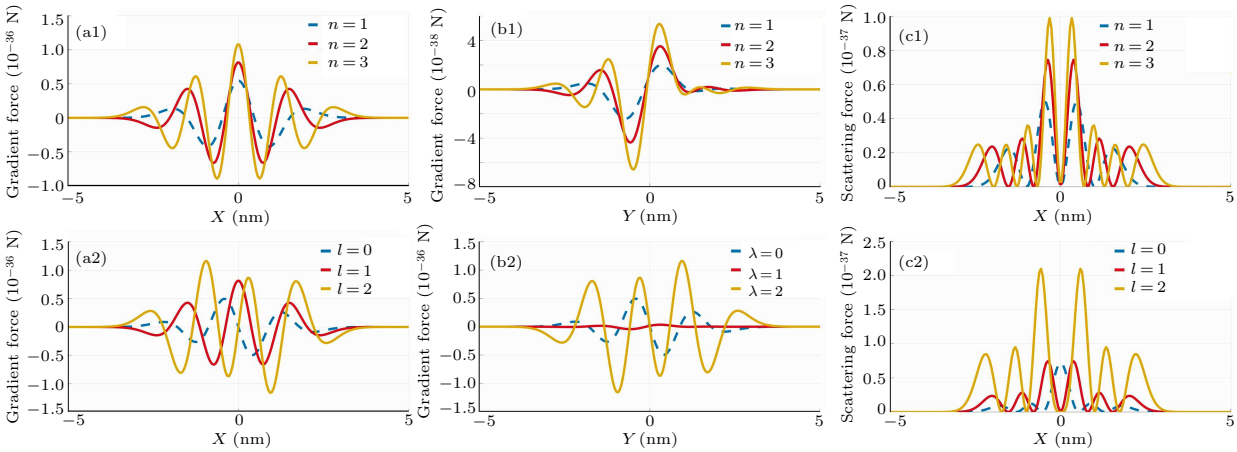


Fig. 6. (a1)–(b1) and (a2)–(b2) are the gradient forces, and (c1)–(c2) are the scattering forces of different parameters of the CPLGST wave packets. $C_1 = 0.5$, $C_2 = 0.5$, $l = 1$ in (a1)–(c1), $n = 1, 2, 3$. $n = 2$ in (a2)–(c2), $l = 0, 1, 2$.

Finally, we demonstrate the characteristics of the gradient force and scattering force of the CPLGST beam under different parameter conditions. When the angular mode number is held constant, the amplitude of the gradient force rises markedly and its fluctuation frequency accelerates with the increase of the radial mode number, showing an asymmetric distribution along the Y-direction and a symmetric distribution along the X-direction, as depicted in Figs. 6(a1) and 6(b1). Meanwhile, a greater radial mode number elevates the peak intensity of the scattering force, increases the number of peak points in its spatial distribution, and enhances the prominence of energy concentration and spatial oscillation characteristics, enabling the light field to exert multi-point directional thrust on particles, as shown in Fig. 6(c1). As illustrated in Figs. 6(a2) and 6(b2), when the radial mode number is fixed, the vibrational structure of the gradient force grows increasingly complex with rising angular mode number, manifested by more oscillations of the fluctuation curve and a greater number of local extreme points. However, it exhibits no symmetric structure in either the X or Y directions. Compared with Fig. 6(c1), the scattering force peaks in Fig. 6(c2) undergo more significant changes with the variation of the angular mode number, with greater fluctuations in peak intensity and more pronounced spatial shifts of peak positions while maintaining an overall symmetric distribution. In summary, the gradient force displays a positive-negative alternating oscillatory distribution in both the X and Y directions, reflecting the bidirectional traction-repulsion gradient effect of the light field on particles in two-dimensional space, while the scattering force is dominated by positive peaks corresponding to the directional scattering thrust exerted by the light field on particles. Although the gradient force of the CPLGST wave packets exhibits an oscillatory distribution with alternating positive and negative values, the positive gradient-force regions form a regular multi-focal potential well structure rather than irregular mechanical oscillations, while the negative gradient-force regions act as potential barriers that enable fixed-point trapping of micro-nano particles; the scattering force presents a directional peak distribution and forms a dynamic mechanical equilibrium with the gradient force, which effectively counteracts the particle escape tendency without inducing trapping instability. Meanwhile, the CPLGST wave packets are composed of coupled Laguerre modes and chirped Pearcey pulses, whose spatial and temporal coherence is guaranteed by the fixed relationship between the phase term $\mathrm{i}l\theta$ and the chirp phase, so that the mechanical field distribution maintains regular coherence without spurious force peaks, further ensuring the stability of particle trapping. The intrinsic mechanism underlying the regulation of optical force characteristics by the radial and azimuthal mode numbers lies in the modulation of the optical field intensity and phase distribution. These field properties are directly mapped to quantitative changes in the mechanical response via the optical force formula. Specifically, increasing the radial mode number raises the number of spatial rings of the Laguerre mode and enhances the radial oscillation frequency of the optical field intensity. This directly increases the fluctuation frequency of the gradient force and the number of scattering force peaks. On the other hand, increasing the azimuthal mode number distorts the spiral phase distribution of the optical field and breaks its spatial symmetry. As a result, the gradient force loses its symmetrical structure in the X and Y directions and exhibits more local extrema, while the scattering force peaks undergo obvious spatial shifts and intensity fluctuations. Notably, this evolutionary law can be rigorously verified through quantitative derivation from the optical intensity distribution and the optical force formula, rather than being only a phenomenological description. Compared with the traditional Laguerre beam trapping technique, the CPLGST wave packets show significant advantages in optical force manipulation: traditional Laguerre beams can only form a single gradient-force potential well and realize the trapping and rotational manipulation of a single particle with a single manipulation dimension, whereas the multi-peak optical force distribution of the CPLGST wave packets forms an

ordered array of multi-focal potential wells, enabling simultaneous fixed-point trapping and multi-dimensional cooperative manipulation of multiple particles, and the number, distribution and intensity of the optical force potential wells can be precisely tailored by flexibly adjusting the radial and azimuthal mode numbers and the second-order chirp factor to meet the manipulation requirements of micro-nano particles with different sizes and arrangements. In addition, the optical force field of the CPLGST wave packets can be dynamically tuned through the synergistic control of dispersion and chirp, while the optical force field of traditional Laguerre beams is statically distributed, resulting in much lower manipulation flexibility. This result provides a critical design basis for realizing precise capture and multi-dimensional manipulation of micro-nano particles, and can be further extended to applications such as medical cell sorting and optical tweezers technology. The CPLGST wave packets outperform conventional Laguerre–Gaussian and Pearcey-based wave packets in optical force efficiency. Their multi-peak optical force distribution enables multi-dimensional particle manipulation and overcomes the limitation of single-particle manipulation.[45]

4. Conclusion

In conclusion, the CPLGST wave packets investigated in this study exhibit superior propagation characteristics in linear dispersive media. Our findings demonstrate that with the azimuthal mode number held constant, an increase in the radial mode number results in a more dispersed radial energy distribution of the CPLGST wave packets, a greater number of concentric rings, and an expanded spatial coverage. In contrast, when the radial mode number is fixed, an increase in the azimuthal mode number converts the central bright spot into a closed bright ring while reinforcing the spiral architecture of the CPLGST wave packets. Moreover, tuning the second-order chirp factor and dispersion parameters can elicit pronounced spatial displacement and splitting behaviors of the wave packets. Notably, this study reveals that the temporal and intensity evolution characteristics of the CPLGST wave packets are synergistically modulated by the second-order chirp factor and the dispersion coefficient, while the propagation direction of these wave packets is determined by the sign of the product of these two parameters. A positive product corresponds to propagation in the negative T-axis direction, whereas a negative product corresponds to propagation in the positive T-axis direction. Specifically, under anomalous dispersion conditions, the peak intensity of the CPLGST wave packets with a negative second-order chirp factor increases significantly, whereas under normal dispersion conditions, the peak intensity of those with a positive second-order chirp factor rises markedly. This offers a robust framework for high-power laser pulse compression. In terms of mechanical properties, the gradient and scattering forces of the CPLGST beams exhibit multi-peak and structurally complex oscillatory characteristics. This unique mechanical force distribution opens up new avenues for microparticle and nanoparticle manipulation as well as the optimization of optical tweezers technology. Taken together, these distinctive properties of the CPLGST wave packets provide important theoretical support and promising application potential for technological innovations in fields such as optical communications and precision manufacturing.

Data availability statement

Data underlying the results presented in this paper are available upon reasonable request.

Acknowledgements

We acknowledge the support from the National Natural Science Foundation of China (Grant Nos. 12204278, 12474294, 12074224, and 12174122), the Natural Science Foundation of the Shandong Province (Grant Nos. ZR2024QA019, ZR2025MS72, ZR2021YQ02, and ZR2020MA087), Young Talent of Lifting Engineering for Science and Technology in Shandong (Grant No. SDAST2025 QTB038), and the Taishan Scholars Program of the Shandong Province (Grant No. tsqn202507178).

References

[1] Forbes A, de Oliveira M and Dennis M R 2021 *Nat. Photonics* **15** 253
[2] He C, Shen Y J and Forbes A 2022 *Light Sci. Appl.* **11** 205
[3] Otte E and Denz C 2020 *Appl. Phys. Rev.* **7** 041308
[4] Yang Y J, Ren Y X, Chen M Z, Arita Y and Rosales-Guzmán C 2021 *Adv. Photonics* **3** 034001
[5] Ma J P, Hu X Q, Wu Y and Wang J G 2025 *Chin. Phys. B* **34** 103301
[6] Shen Y J, Wang Z Y, Fu X, Naidoo D and Forbes A 2020 *Phys. Rev. A* **102** 031501
[7] Graffitti F, D'Ambrosio V, Proietti M, Ho J, Piccirillo B, de Lisio C, Marrucci L and Fedrizzi A 2020 *Phys. Rev. Res.* **2** 043350
[8] Allen L, Beijersbergen M W, Spreeuw R J C and Woerdman J P 1992 *Phys. Rev. A* **45** 8185
[9] He H, Friese M E J, Heckenberg N R and Rubinsztein-Dunlop H 1995 *Phys. Rev. Lett.* **75** 826
[10] Friese M E J, Enger J, Rubinsztein-Dunlop H and Heckenberg N R 1996 *Phys. Rev. A* **54** 1593
[11] Simpson N B, Dholakia K, Allen L and Padgett M J 1997 *Opt. Lett.* **22** 52
[12] Li Y, Zhou L M and Zhao N 2021 *Opt. Lett.* **46** 106
[13] O'Neil A T, MacVicar I, Allen L and Padgett M J 2002 *Phys. Rev. Lett.* **88** 053601
[14] Kovalev A A, Kotlyar V V and Porffrev A P 2016 *Opt. Lett.* **41** 2426
[15] Siviloglou G A, Broky J, Dogariu A and Christodoulides D N 2007 *Phys. Rev. Lett.* **99** 213901
[16] Siviloglou G A and Christodoulides D N 2007 *Opt. Lett.* **32** 979
[17] Ring J D, Lindberg J, Mourka A, Mazilu M, Dholakia K and Dennis M R 2012 *Opt. Express* **20** 18955
[18] Deng D M, Chen C D, Zhao X, Chen B, Peng X and Zheng Y S 2014 *Opt. Lett.* **39** 2703
[19] Manousidaki M, Papazoglou D G, Farsari M and Tzortzakis S 2016 *Optica* **3** 525
[20] Panagiotopoulos P, Papazoglou D G, Couairon A and Tzortzakis S 2013 *Nat. Commun.* **4** 2622

[21] Panagiotopoulos P, Abdollahpour D, Lotti A, Couairon A, Faccio D, Papazoglou D G and Tzortzakis S 2012 *Phys. Rev. A* **86** 013842
[22] Zhang L P, Deng D M, Yang X B, Wang G H and Liu H Z 2020 *Opt. Express* **28** 425
[23] Zhang L P, He S L, Peng X, Huang L Q, Yang X B, Wang G H, Liu H Z, He Y J and Deng D M 2021 *Chaos Soliton. Fract.* **143** 110608
[24] Zang X, Dan W S, Wang F, Zhou Y M, Xu Y Q and Zhou G Q 2022 *Opt. Express* **30** 24948
[25] Wu Y, Zhao J J, Lin Z J, Huang H Q, Xu C J, Liu Y J, Chen K H, Fu X M, Qiu H X, Liu H Z, Wang G H, Yang X B, Deng D M and Shui L L 2021 *Opt. Lett.* **46** 2461
[26] Li S B and Jiang X T 2025 *Opt. Commun.* **598** 132395
[27] Kondakci H E and Abouraddy A F 2019 *Nat. Commun.* **10** 929
[28] Yessenov M and Abouraddy A F 2020 *Phys. Rev. Lett.* **125** 233901
[29] Liang Z H, Liu Y J, Luo Y J, Chen H C and Deng D M 2023 *Opt. Lett.* **48** 2543
[30] Chen C D, Zhang L P, Yang S, Li S Y and Deng D M 2024 *Opt. Lett.* **49** 2681
[31] Zhang L P, Zhang X, Yu P X, Ge X L, Chen C D, Man Z S and Deng D M 2024 *Opt. Lett.* **49** 4681
[32] Xu G F, Liu Y F, Ouyang J Y, He S L, He Y J, Zhao F, Zheng Y B, Deng D M and Peng X 2025 *Opt. Express* **33** 5746
[33] Peng X, Ouyang J Y, Xu D L, He S L, Mo Z W, Qiu Y L, He Y J, Zhao D M and Deng D M 2022 *Opt. Express* **30** 6193
[34] Wang C, Liang Z H, Ruan Z, Ma M X and Deng D M 2025 *Opt. Lett.* **50** 4114
[35] Luo Y J, Liang Z H, Mo Z W, Shi J Y, Huang J H, Yang Y Z, Lin X J, Ruan Z, Wang C and Ouyang M 2024 *Opt. Lett.* **49** 290
[36] Chong A, Renninger W H, Christodoulides D N and Wise F W 2010 *Nat. Photonics* **4** 103
[37] Kshirsagar B and Koser A A 2019 *AIP Conf. Proc.* **2100** 020200
[38] Zhou G Q, Wang F and Feng S S 2020 *Opt. Express* **28** 19683
[39] Luan K C, Li S Y, Zhang X C, Zhang X, Chu Y H, Man Z S, Ge X L, Li H J, Fu S G, Chen C D and Zhang L P 2025 *Opt. Commun.* **592** 132233
[40] Yang S, Yu P X, Xu Z, Zhang X C, Luan K C, Ge X L, Lei C X, Chen C D, Man Z S and Zhang L P 2025 *Nonlinear Dyn.* **113** 23473
[41] Zhang Z J, Wu Y J, Tao M, Wang W T, Xu Z H, Sun Z Y, Zhuang C H, Liu Z H and Deng D M 2025 *Opt. Laser Technol.* **188** 112886
[42] Zhou W J, Liu A X, Huang X W, Bai Y F and Fu X Q 2022 *J. Opt. Soc. Am. A* **39** 736
[43] Peng X, Peng Y L, Li D D, Zhang L P, Zhuang J L, Zhao F, Chen X Y, Yang X B and Deng D M 2017 *Opt. Express* **25** 13527
[44] Chen X P, Xu C J, Yang Q, Luo Z M, Li X X and Deng D M 2020 *Chin. Phys. B* **29** 064202
[45] Liang Y, Tan L, Liu N N, Chen K J, Liang H P, Wu H H, Luo B S, Lu F X, Chen H H, Zou B S and Hong P L 2023 *Phys. Rev. Appl.* **19** 014016